Original Article

Enhancing joint strength of bobbin tool friction stir welded Al–Mg–Si alloy via post-weld aging process

C. Yang [a,b], Z.L. Wang [a], M. Zhang [a], P. Xue [a], F.C. Liu [a], D.R. Ni [a,c,*], B.L. Xiao [a], Z.Y. Ma [a,**]

[a] Shi-changxu Innovation Center for Advanced Materials, Chinese Academy of Sciences, 72 Wenhua Road, Shenyang 110016, China
[b] School of Materials Science and Engineering, Shenyang University of Technology, 111 Shenliao West Road, Shenyang 110870, China
[c] Binzhou Institute of Technology, Shandong Key Laboratory of Advanced Aluminium Materials and Technology, Weiqiao-UCAS Science and Technology Park, Binzhou, Shandong Province 256606, China

ABSTRACT

For the precipitation-strengthened aluminum alloys such as Al–Mg–Si alloys, the friction stir welded (FSW) joints produced with T6-treated plates usually exhibit obvious softening in the heat-affected zones (HAZ), significantly reducing the joint strength. When bobbin tool FSW (BT-FSW) is used, severer softening of the HAZ occurred compared to conventional FSW. It is therefore crucial to achieve precipitate morphology control in the HAZ for BT-FSW through original plate state selecting, welding parameter optimizing, and post-weld artificial aging (PWAA). Compared to the conventional welding process (plates welded directly under T6 condition, T6-BT), in the present work, a post-weld aging process was proposed: the plates under T4 condition were BT-FSWed using optimizing parameters (T4-BT), and then subjected to PWAA (T4-BT-PWAA). The intrinsic microstructural differences between the T6-BT and T4-BT-PWAA joints were revealed. More attentions were paid on the microstructural evolution in the lowest hardness zone (LHZ) during PWAA for the T4-BT joint. The LHZ of the T6-BT joint exhibited an over-aged state characterized by coarsened β' phase and the hardness in this zone had very limited enhancing space when subjected to post-weld peak aging. For the T4-BT joint, the LHZ was characterized by a low density of precipitates and presented excellent re-precipitating ability of β'' phase during PWAA, with the ultimate tensile strength increased by ~11.4% compared to its T6 counterpart, which is very beneficial for engineering applications.

* Corresponding author.
** Corresponding author.
E-mail addresses: drni@imr.ac.cn (D.R. Ni), zyma@imr.ac.cn (Z.Y. Ma).

Abbreviations

BT-FSW	Bobbin tool friction stir welding
HAZ	Heat-affected zone
LHZ	Lowest hardness zone
TMAZ	Thermal-mechanically affected zone
NZ	Nugget zone
PWAA	Post-weld artificial aging
T6-BT	plates welded directly under T6 condition
T4-BT	plates welded directly under T4 condition
T4-BT-PWAA	plates welded under T4 condition followed by PWAA
T6-BT-PWAA	plates welded under T6 condition followed by PWAA

1. Introduction

Friction stir welding (FSW), as a solid state welding technique for joining Al alloys invented by The Welding Institute (TWI) in 1991 [1], has over years been widely applied in various industries, such as aerospace, transportation and shipping, etc. For meeting varied industrial requirements, process variants are developed to acquire specific microstructures [2—4].

Despite the advantages of the conventional FSW (C-FSW) in joining aluminum alloys, the bottom defects, such as lack of penetration and kissing-bond, are inclined to generate when the welding parameters are improperly set; moreover, high quality welding of complex shaped hollow extrusions is difficult to achieve with the C-FSW because of shape limit and large axial forging load in the process. As a result, bobbin tool FSW (BT-FSW) has been developed to overcome those disadvantages. In recent years, much attention hence has been paid to BT-FSW based on its special characteristics [5—11]. Among the reports, BT-FSW joints of precipitation-strengthened Al alloys are usually produced with T6-treated plates [12—15], where the HAZ has more severe softening than that of C-FSW joints. It has been well documented that the hardness and strength of precipitation-strengthened Al alloys are dominated by precipitate evolution. For their FSW joints, HAZ, characterized by the dissolution/coarsening of the precipitates, is the weakest zone dominating the strength of the whole joint. Therefore, reducing the softening of the HAZ by controlling the precipitate dissolution/coarsening becomes a key to enhance the FSW joints of precipitation-strengthened Al alloys. Based on the previous studies, this can be achieved by decreasing the duration at high temperature of the thermal cycles in the HAZ, which could alleviate the precipitate dissolution/coarsening.

In our previous study [16], strength enhancement of the BT-FSW 6061Al joint was achieved by increasing the welding speed to reduce the duration at high temperature of the thermal cycles, to restrain the precipitate dissolution/coarsening in the HAZ. Nevertheless, the strength enhancement was limited. The proper post-weld heat-treatment is supposed to be an effective method. Unfortunately, when conducting the conventional post-weld solid solution (PWSS)

treatment, abnormal grain growth might occur in the nugget zone (NZ) for the FSW joints, reducing the joint properties [17,18]. Hence, the post-weld artificial aging (PWAA) without foregoing PWSS is expected to be an optimal process. Attempts are taken to enhance the joint strength in the BT-FSW of 6082Al-T6 alloy by underwater welding [14] and post-weld aging [15]. In the case of underwater welding, the HAZ was still characterized by coarse precipitates and the increment was limited. As for the study of post-weld aging, the BT-FSW joint was subjected to post-weld natural aging (PWNA) and PWAA, whereas the joint strength decreased in both the aging processes due to the coarsening of precipitates in the HAZ when subjected to BT-FSW in T6 condition.

It should be pointed out that different precipitate states of the HAZ would exhibit different PWAA responses, thereby producing different joint strength enhancements. Sato et al. [19] showed that in a FSW 6063 aluminum alloy joint, the zones with precipitate dissolution could achieve hardness recovery through PWAA, while the zones where precipitates coarsened could hardly gain hardness increase. Therefore, it is crucial to produce a HAZ with excellent re-precipitating ability in the BT-FSW joint.

In the present work, a process of BT-FSW under T4 condition (T4-BT) followed by PWAA, was proposed. The aim is to (a) enhance the properties of BT-FSW 6061Al joints by controlling the precipitation status of the HAZ and (b) elucidate the precipitation evolution characteristics during welding thermal cycle and PWAA processes.

2. Experimental

The as-received base material (BM) was 6.35 mm thick 6061Al-T4 plates (Al—Mg—Si alloy) with dimensions of 320 mm × 80 mm. Part of the plates were subjected to T6 treatment (solid solution treated at 530 °C for 0.5 h, water quenched, and then aged at 175 °C for 12 h) for comparative experiment. The chemical compositions of the BM are listed in Table 1.

BT-FSW was performed on the T4-/T6-treated plates using a numerically controlled FSW machine (FSW-5LM-020) and the welding direction was parallel to the rolling direction of the BM. The tilt angle of the welding tool was 0° in the welding process. The bobbin tool used in the experiment was made of H13 steel, which consisted of symmetrical upper and lower shoulders with a scrolled groove feature. The shoulders were 22 mm in diameter and were connected by a cylindrical pin with a mixed thread 8 mm in diameter. The fixed gap between the shoulders was 6 mm which indicated the pin length. The figure of the welding tool is presented in Fig. 1a. The rotation rate and welding speed were optimized as 600 rpm and 150 mm/min respectively in the present work based on a previous study [16]. The post-weld aging of the joints was

Table 1 — Chemical composition of 6061Al BM (wt.%).

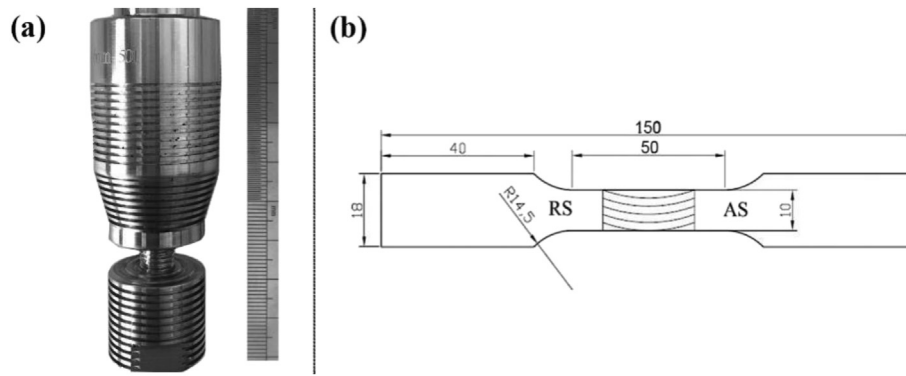| Mg	Si	Cu	Zn	Fe	Mn	Cr	Ti	Al
1.01	0.45	0.22	0.04	0.70	0.15	0.08	0.15	Bal.

Fig. 1 – Configuration and size of (a) bobbin tool and (b) tensile specimen.

conducted at 175 °C for various durations of time. The joints were kept for two weeks prior to post-weld aging.

Microstructural observations were conducted using optical microscopy (OM, Axiovert 200 MAT), scanning electron microscopy (SEM, ZEISS SUPRA 55), transmission electron microscopy (TEM, Thermo Fisher Talos F200x) and electron backscattered diffraction (EBSD, HKL Channel 5 System). OM specimens were prepared by grinding, polishing, and etching with Keller's reagent (HNO$_3$: HCl: HF: H$_2$O = 2.5: 1.5: 1: 95 vol%). Twin-jet electro-polishing was used to prepare TEM samples with a 30% nitric acid and 70% methanol solution (temperature: 30 °C; voltage: 15 V). Specimens for EBSD were prepared by grinding and mechanical polishing, followed by electropolishing in a solution of 10% perchloric acid and 90% alcohol solution at −25 °C and 15 V for 1 min. The differential scanning calorimetric (DSC) experiment was conducted with a DSC204F1 type instrument. The DSC specimens were cut into 3 mm diameter disks with a thickness of 1 mm in specific zones and then mechanically-polished to get rid of surface oxides. The specimens were then subjected to DSC experiment at a heating rate of 10 °C/min from room temperature to 500 °C to detect the precipitate evolution.

An auto testing machine (Leco, LM-247AT) was used for hardness measurement on the cross-section along the center line across the weld under a load of 300 g, holding for 15 s. Tensile specimens with a gauge 50 mm in length and 10 mm in width were machined perpendicular to the welding direction, and the specimen size is shown in Fig. 1b. Room-temperature tensile tests were conducted at a strain rate of 1×10^{-3} s^{-1}. Three specimens were tested for an accurate result. All the FSW samples were kept 1 month before examinations of the microstructure and mechanical properties after FSW.

3. Results

3.1. Microstructures of T4-BT joint

The cross-sectional microstructure of the BT-FSW joint is shown in Fig. 2a. Four typical zones can be seen: NZ, thermal-mechanically affected zone (TMAZ), HAZ and BM. The NZ presented a typical "hour-class" shape. The NZ/TMAZ

boundary was more obvious on the advancing side (AS) than that on the retreating side (RS). The microstructure in the NZ presented a symmetrical feature. Further examination via EBSD showed that the NZ (marked with yellow rectangle in Fig. 2a) was characterized by equiaxed fine grain structures with a mean grain size of ~8.5 μm (Fig. 2b). The percentage of low angle grain boundaries (LAGBs) for the BT-FSW joint was much higher (Fig. 2c) compared with that of C-FSW joint, which was due to the intense plastic deformation induced by the two shoulders.

3.2. Microstructures and mechanical properties of T6-BT joint

Fig. 3 shows the precipitate morphology in the lowest hardness zone (LHZ) located in the HAZ of the T6-BT and T6-BT-PWAA joints. The incident direction of the electron beam was parallel to the $<100>_{Al}$ zone axis of Al matrix for all the images in the present work. As can be seen, a relatively low density of precipitates in three types was clearly observed in the LHZ of the T6-BT joint (Fig. 3a). First, the rod and dot-shaped precipitates were proved to be β', as indicated with white arrows. Second, the platelet-shaped precipitates were proved to be β that were indicated with blue arrows. A few lath-like precipitates as pointed with green arrows could be β' or B' phase, and will be judged with high resolution TEM (HRTEM) examination in the following part. The T6-treated 6061 Al alloy mainly contains β'' as the effective hardening precipitate [20–22]. After FSW, the as-welded LHZ presented a slightly over-aged condition with β' accounting for most of the hardening (Fig. 3a). After the PWAA (Fig. 3b), the number of β' phase (rod-like precipitates) increased with obvious coarsening. Although there were a few β' re-precipitated, the number of β phase increased in the meanwhile.

Both the hardness profiles of the T6-BT and T6-BT-PWAA joints exhibited typical "W" shapes (Fig. 4), with the LHZs located in the HAZs. For the T6-BT joint, the hardness values in the NZ and LHZ were 70.5 ± 1.9 and 56.9 ± 1.9, respectively, whereas the values were 91.3 ± 4.0 and 62.8 ± 0.6 respectively for the T6-BT-PWAA joint. It can be clearly seen that the hardness increment in the NZ was ~20 HV, whereas it was only ~6 HV in the LHZ after PWAA. It apparently showed that
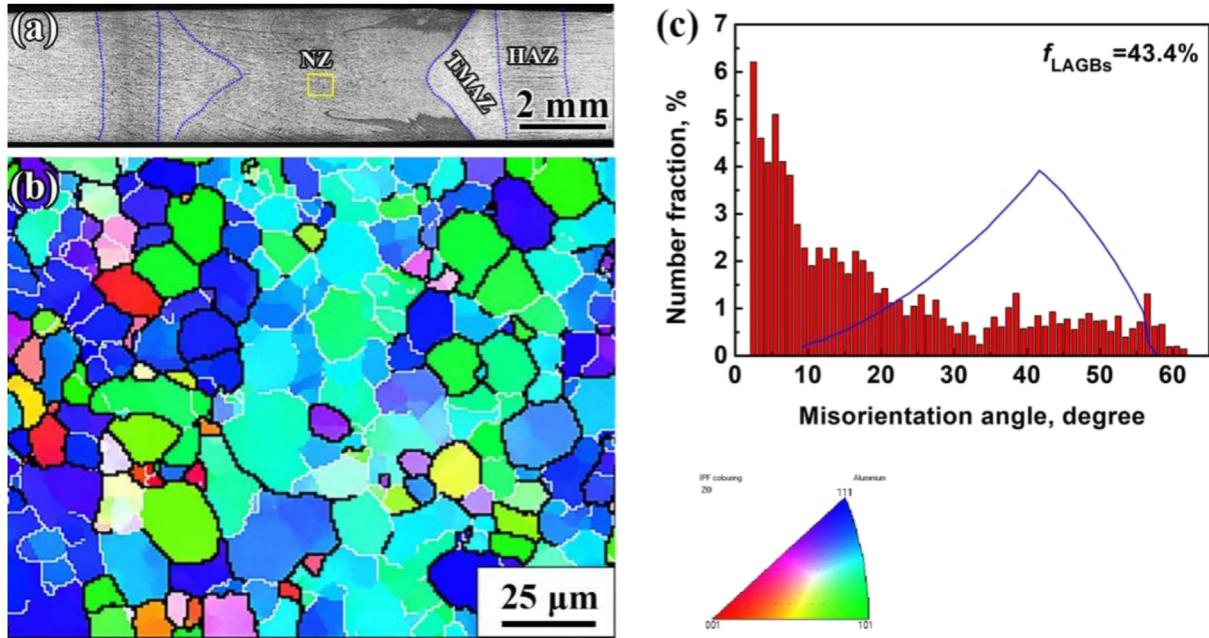
Fig. 2 — Microstructure of T4-BT joint: (a) cross-sectional macrostructure, (b) EBSD map of the NZ center, (c) misorientation angle distribution in the NZ center.

the NZ had remarkable potential to achieve hardness increase whereas the enhancing space was very limited in the LHZ of the T6-BT joint.

3.3.   Precipitation and microhardness evolution of T4-BT joint during PWAA

Fig. 5 presents the hardness profiles of the T4-BT joint subjected to PWAA. The hardness values of all zones in the joint enhanced with increasing the aging time and reached the peak after 12 h (Fig. 5b). The hardness values in the NZ increased from 69.2 ± 0.9 HV under as-welded condition to 90.1 ± 1.4HV under peak condition, whereas the hardness values in the LHZ increased apparently from 58.8 ± 0.2 HV to 75.6 ± 1.1 HV (Fig. 5a and b).

For the T4-BT joint, the hardness increment in the NZ and LHZ were ~21 HV and ~17 HV, respectively. Apparently, the LHZ exhibited a similar enhancing ability as the NZ, and the hardness increment in the LHZ of the T4-BT joint (~17 HV) was remarkably higher than that of the T6-BT joint (~6 HV). With increasing the aging time further, the hardness values kept nearly constant and then decreased slightly at 48 h (Fig. 5c).

To reveal the hardness evolution tendency of different zones, the aging kinetics curves of the BM, NZ and LHZ on the AS are shown in Fig. 6. The curves revealed several findings. Firstly, the hardness values in all the three zones increased obviously with aging time in the early stage of aging (0−4 h), then increased slowly until reached the peak value after 12 h (peak aging, PA). Secondly, the curves of the BM and NZ displayed similar profiles. With prolonging the aging time
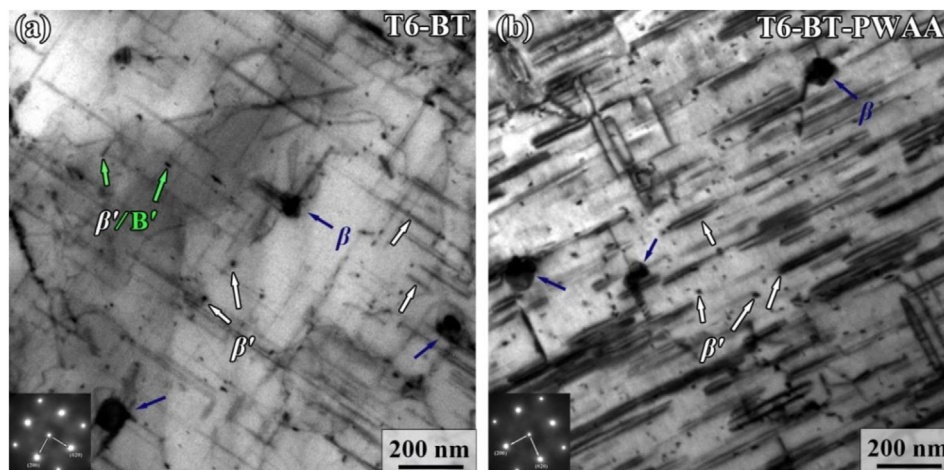

Fig. 3 — TEM images showing precipitates in the LHZ of (a) T6-BT joint and (b) T6-BT-PWAA joint.
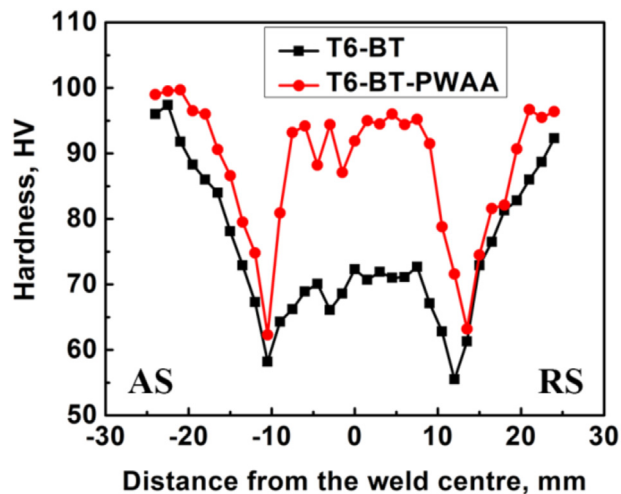
Fig. 4 − Hardness profiles of joints produced with T6-treated BM (AS: advancing side, RS: retreating side).

slowly in the early stage and decreased obviously until reaching 48 h, demonstrating that the LHZ had lower precipitation hardening rate in the early stage and lower thermal stability in the over-aged stage.

In order to reveal the intrinsic factor that led to the apparent increment of hardness in the LHZ, the bright-field TEM images of the precipitates at specific aging time are shown in Fig. 7. The T4-BT LHZ consisted of low density of rod-like (β'), dot-like (β') and lath-like (B') precipitates, which are typical post-β'' phases in over-aged condition [21,23]. With prolonging the aging time, the number of the precipitates increased and the rod-like ones grew further with some fine dot- and lath-like ones re-precipitating. When reaching the PA condition (12 h), the precipitates exhibited a high density. The fine dot-like ones (β'') re-precipitated and were distributed among the β' precipitates, and some of β' grew further in size (Fig. 7d). At 48 h, most of β' precipitates transformed into stable β with some β' being remained. The types of the precipitates will be identified with HRTEM examination in the following part.

Fig. 8 shows the precipitation evolution of the as-received T4-treated BM with aging time. The as-received BM was almost solid solution condition with few precipitates visible (Fig. 8a). After artificial aging, the precipitating occurred and
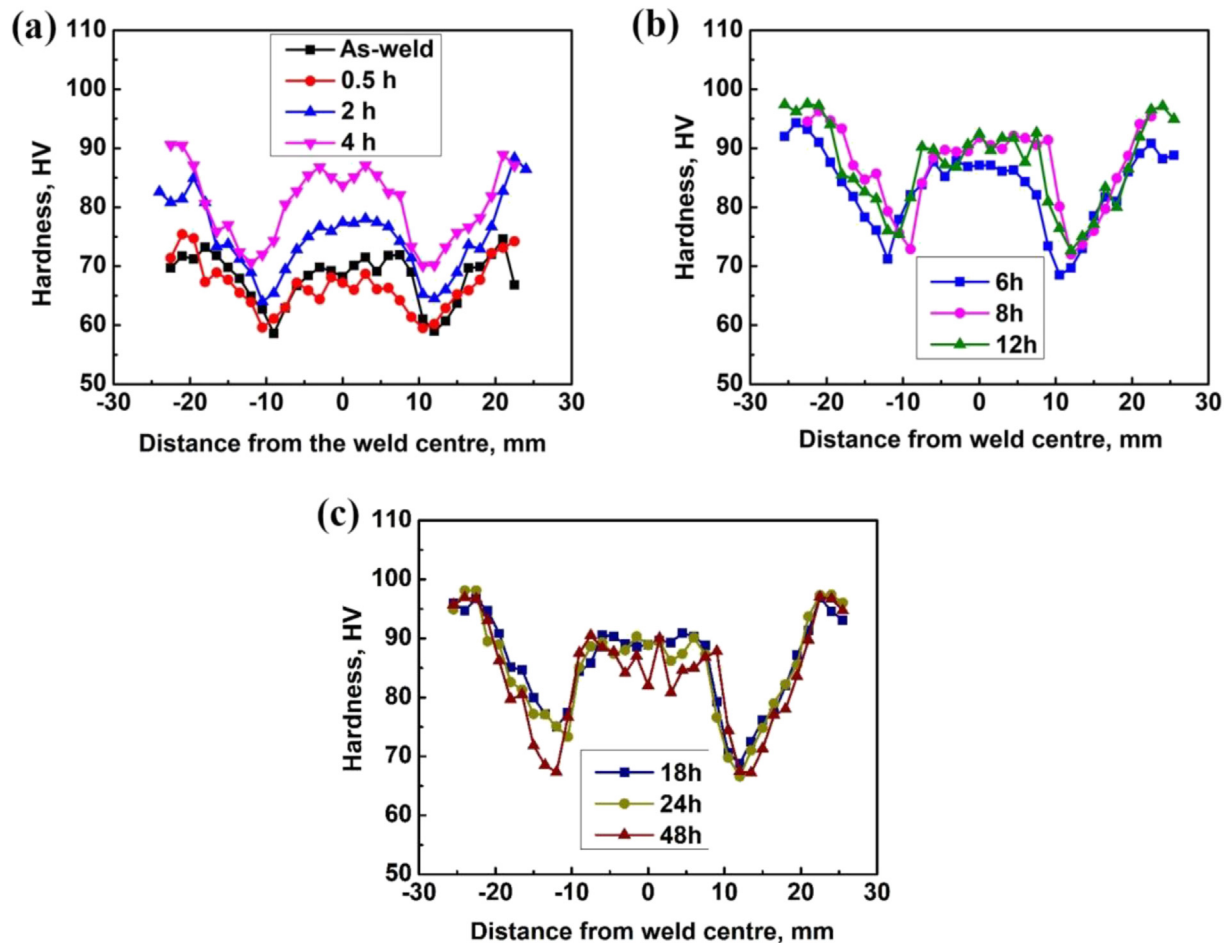
further, the hardness kept nearly constant till 48 h for the BM but decreased slightly for the NZ, which indicated that the BM had higher thermal stability. Thirdly, the hardness increased

Fig. 5 − Microhardness profiles of T4-BTjoint after various aging times: (a) as-weld and early stage of aging; (b) 6 h−12 h; (c) 18 h−48 h.
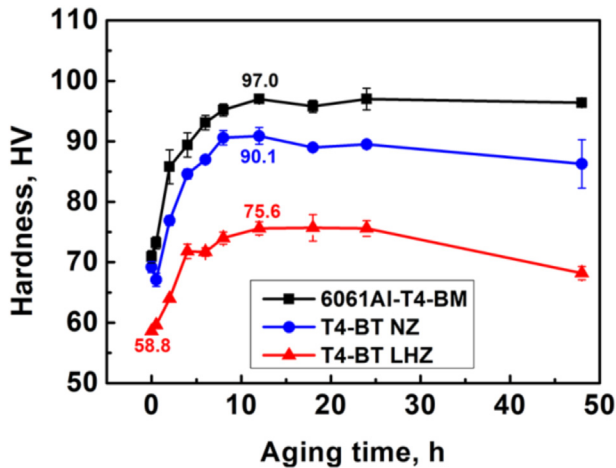
Fig. 6 — Aging kinetics curves of different zones in the T4-BT joint.

fine dot-like precipitates can be observed at 2 h (Fig. 8b). In the case of prolonged aging time, the number of the fine needle-shaped and dot-like precipitates (β'') increased and reached the peak at 12 h (Fig. 8d), which corresponded to the highest hardness value. When surpassing 12 h, a part of β'' precipitates began to grow and some coarsened ones can be observed at 48 h (Fig. 8e). However, the coarsening extent was much lower than that of the T4-BT LHZ at over-aged condition, showing a high thermal stability from the microstructural view.

3.4. Tensile properties

The UTS of the T4-BT, T4-BT-PWAA and T6-BT joints were 207 MPa, 235 MPa and 211 MPa, respectively, as determined from the engineering stress-strain curves in Fig. 9. It can be seen that the UTS of T4-BT joint increased from 207 MPa to 235 MPa after 12 h PWAA, which was ~24 MPa higher than that of T6-BT joint. The UTS of T4-BT and T6-BT joints were at the same level.

Fig. 10 presented the fracture locations of the joints under different conditions. The tensile strain concentrated in the LHZs during the tensile process and obvious necking was observed. As the deformation continued, the fracture occurred in the LHZs, which corresponded well with the hardness values.

4. Discussions

4.1. Microstructural characteristics

The precipitation evolution of FSW Al–Mg–Si alloys is closely related to the original condition of the plates and the welding process [24]. In the C-FSW of Al alloys, the HAZ usually went through thermal cycles with a peak temperature around 370 °C [21,25]. Though investigations associated with FSW of Al–Mg–Si alloys [24,26] claimed the similar softening effect in the HAZ of the joints produced with T6-and T4-treated plates,
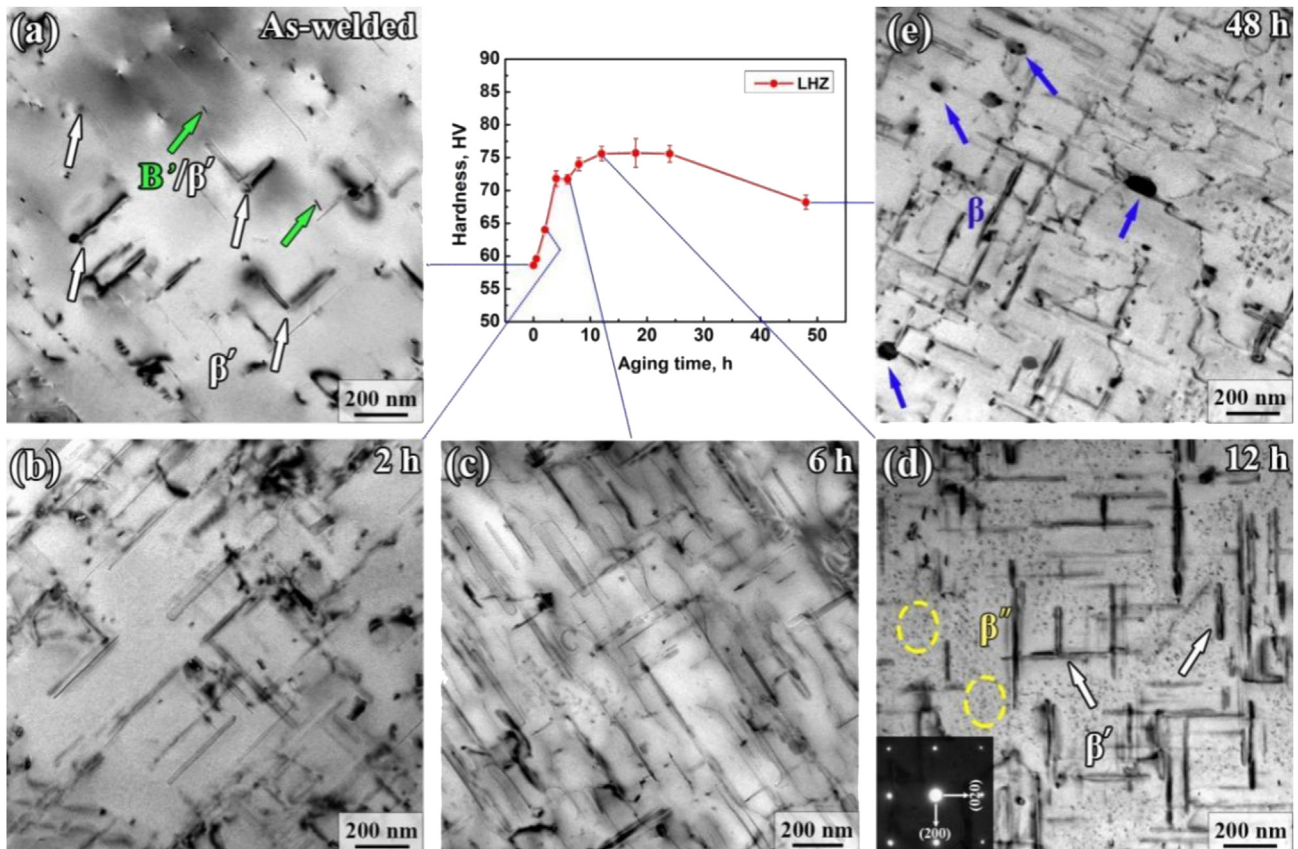

Fig. 7 — TEM images showing precipitates evolution in LHZ of T4-BT joint with aging time.
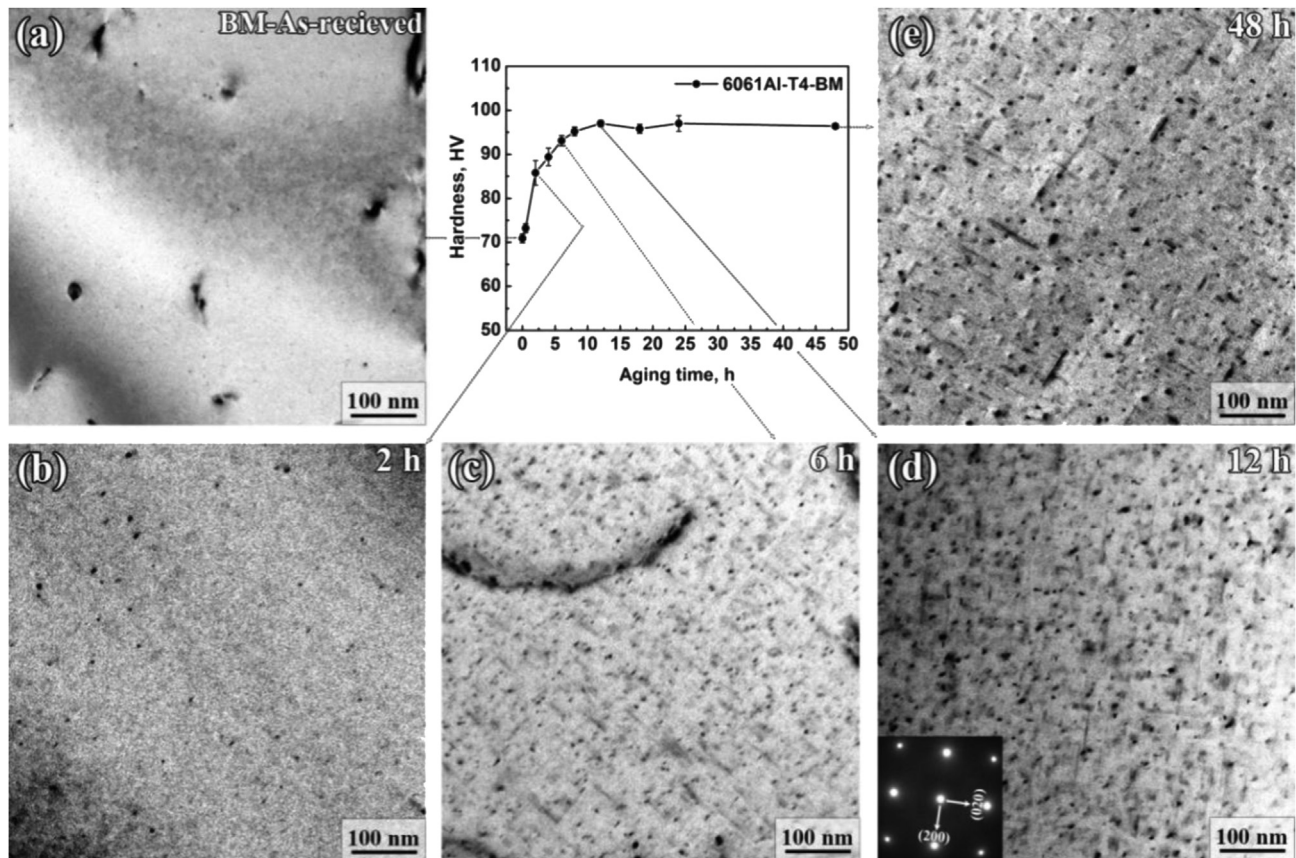
Fig. 8 – TEM images showing precipitates evolution of 6061Al-T4 BM with aging time.

few demonstrated the intrinsic microstructural differences between the two kinds of joints.

As mentioned above, the T6-BT joint was produced with the plates that was characterized by β'' phase. As a result, the precipitates in the T6-BT LHZ experienced complex evolution and finally was dominated by β' phase, and exhibited an over-aged status (Fig. 3a). As for the T4-BT joint, it was produced with the T4-treated BM that was almost solid solution

Fig. 9 – Engineering stress-strain curves of various joints.

condition. Part of the clusters, formed during natural aging, dissolved and the remaining part transformed into coarsened β' phase in the LHZ during the BT-FSW thermal cycles. As a result, the LHZ with a much lower density of precipitates (Fig. 7a) was acquired. It can be seen that the softening in the LHZ was caused by the coarsened β' phase for the T6-BT joint, whereas it was mainly due to the low density of precipitates for the T4-BT joint.

The DSC analysis (Fig. 11) was conducted for the 6061Al-T4 BM, NZ and LHZ in the T4-BT joint to further unveil the precipitation behavior in the thermal process of specific zones. Three exothermic peaks were clearly seen, which were correlated to different precipitation behaviors. Exothermic peak I (around 260 °C) was well reported to be the fine needle-shaped β'' precipitation [21,27]. Exothermic peak II (~300 °C) indicated the formation of short rod-like β' and lath-like B' phases and exothermic peak III (around 350 °C) was associated with the β precipitation [21].

A further look into the curves showed that the peak I (β'' precipitation peak) in the curve of the LHZ had a smaller peak area and a delayed precipitating process (~270 °C) compared to the other two zones, which indicated a weak aging kinetics at early stage. The weak aging kinetics can be clearly seen from the aging kinetics curve at the early stage (Fig. 6). For the BM and T4-BT NZ, there was an endothermic peak (~220 °C) prior to peak I, which indicated the dissolution of G.P. zones [28]. Peak II was observed only in the BM and NZ, which indicated that β' precipitation occurred in this two zones during PWAA.
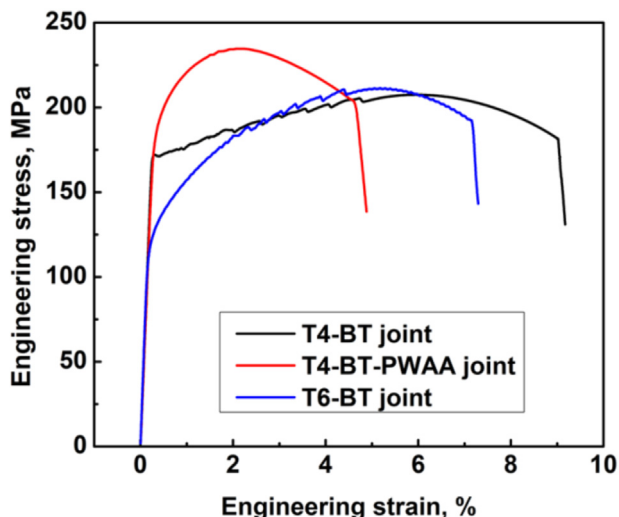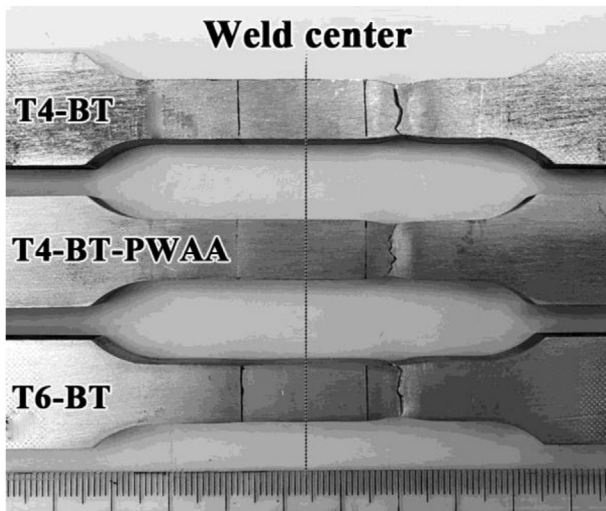
Fig. 10 – Fracture locations of the joints under different conditions.

However, for the LHZ, the β' precipitation peak area (peak II) can hardly be seen, which indicated no β' phase transformation. That is to say, in as-welded LHZ, almost no β'' phases would transform into β' phases in the DSC test, because the thermal cycles during welding led to the formation of β' phases prior to DSC testing. Peak III consisted of two continuous peaks from 350 °C to 370 °C for the BM and T4-BT NZ, which indicated a wide range of the β formation. As for LHZ, only one smaller peak around 350 °C was observed, revealing a small amount of β formation.

For 6000 series Al alloys in solid solution condition, four exothermic peaks are usually observed at ~85 °C, ~250 °C, ~300 °C and ~370 °C, associated with the formation of G.P. zone, β'', β' and β phases, respectively [29]. However, no exothermic peaks were observed around 85 °C in the LHZ in the T4-BT joint, which indicated that the formation of G.P. zones has finished at T4 and T4-BT conditions.
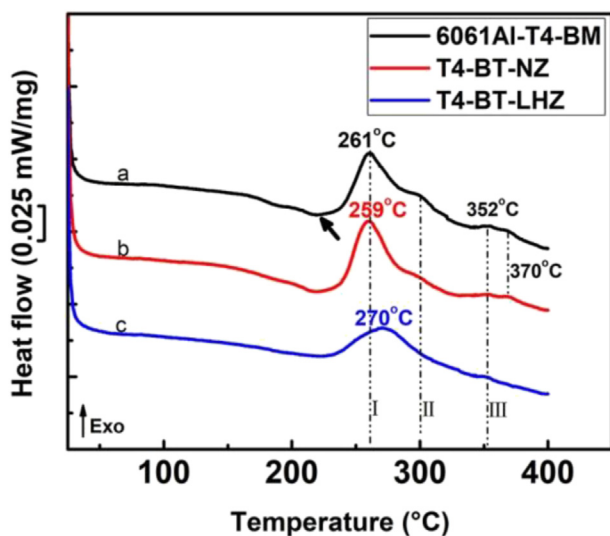

Fig. 11 – DSC curves at a heating rate of 10 °C/min for samples of (a) 6061Al-T4 BM, (b) T4-BT NZ, (c) T4-BT LHZ.

4.2. Effect of PWAA on precipitation evolution

The precipitation sequence of a low Cu/Cu-free Al–Mg–Si alloy during aging was well demonstrated in previous works as [21–23]:

SSSS → atomic clusters → G.P. zones → β'' → β', U1, U2, B' → β, Si.

The typical HRTEM images and corresponding Fast Fourier Transformation (FFT) patterns of three types of precipitates are shown in Fig. 12 to confirm the structures of the precipitates in the LHZs of T6-BT, T4-BT and T4-BT-PWAA joints. In the T6-BT (Fig. 3a) and T4-BT LHZs (Fig. 7a), two kinds of phases were detected. The dominant dot-like and rod-like precipitates were identified to be metastable β' phase, which appeared in over-aged condition. It has a hexagonal structure with a unit cell of a = 0.715 nm, c = 0.405 nm and $(100)_{Al}$ habit planes [21,30] (Fig. 12a). The lath-like precipitates were confirmed as B' phase (Fig. 12c), and it also has a hexagonal unit cell of a = 1.04 nm, c = 0.405 nm, γ = 120° and an orientation of $(0001)_B \| (100)_{Al}$. What should be noted was that the B' phase usually coexisted with other post-β'' phases under over-aged condition in a Si-excessive (Mg/Si < 2) Al–Mg–Si alloy [23]. The 6061Al in the present work was Mg-excessive (Mg/Si > 2), thus it was hard for the B' phase to form. The formation of B' phase in the LHZ may be attributed to the rapid diffusion of Si element during the welding process.

A further examination of the T4-BT LHZ in the PA condition indicated that in addition to the above two kinds of phases, the re-precipitated fine dot- and needle-like precipitates were identified as the effective hardening precipitate β'', which was distributed among rod-like β' precipitates (Fig. 7d, marked with yellow circles). It has a C-centered monoclinic unit cell of a = 1.516 nm, b = 0.405 nm, c = 0.674 nm and α = 105.3° [21,30]. The re-precipitating of large numbers of β'' precipitates further proved that the T4-BT LHZ had excellent re-precipitating potential by microstructure control when subjected to PWAA.

For the plates in T6 state, the effective strengthening phase β'' was formed, which was suggested as monoclinic Mg_5Si_6 or $Mg_5Al_2Si_4$ [31,32]. During the BT-FSW process, most of the β'' precipitates transformed directly into β' phase and a few of them dissolved into Al matrix in the LHZ. The thermal cycles in the LHZ would act as a short-time aging with a peak temperature of ~370 °C, and the dissolved β'' phase would re-precipitate as small β' phase promoted by of the thermal cycles. As a result, the LHZ of the T6-BT joint was characterized by β' phase. When subjected to the PWAA, the β' phase coarsened and some transformed into coarse equilibrium β phase to show a well over-aged state (Fig. 3b). Before subjected to the BT-FSW, the T4-treated plates have finished the clustering. After the BT-FSW, the T4-BT LHZ was characterized by only low density of post-β'' phases: β' and B' phases (Fig. 7a).

It was interesting to note that the precipitation sequence in the LHZ during welding could be described as: atom clustering → β', B', omitting β'' formation. As mentioned above, the welding thermal cycles experienced by the LHZ acted as a short-time aging process. After welding, most of the clusters were unstable and redissolved as solute atoms into the Al matrix, and some of the clusters evolved directly into β' and B' phases. This phenomenon was reported in the aging of an
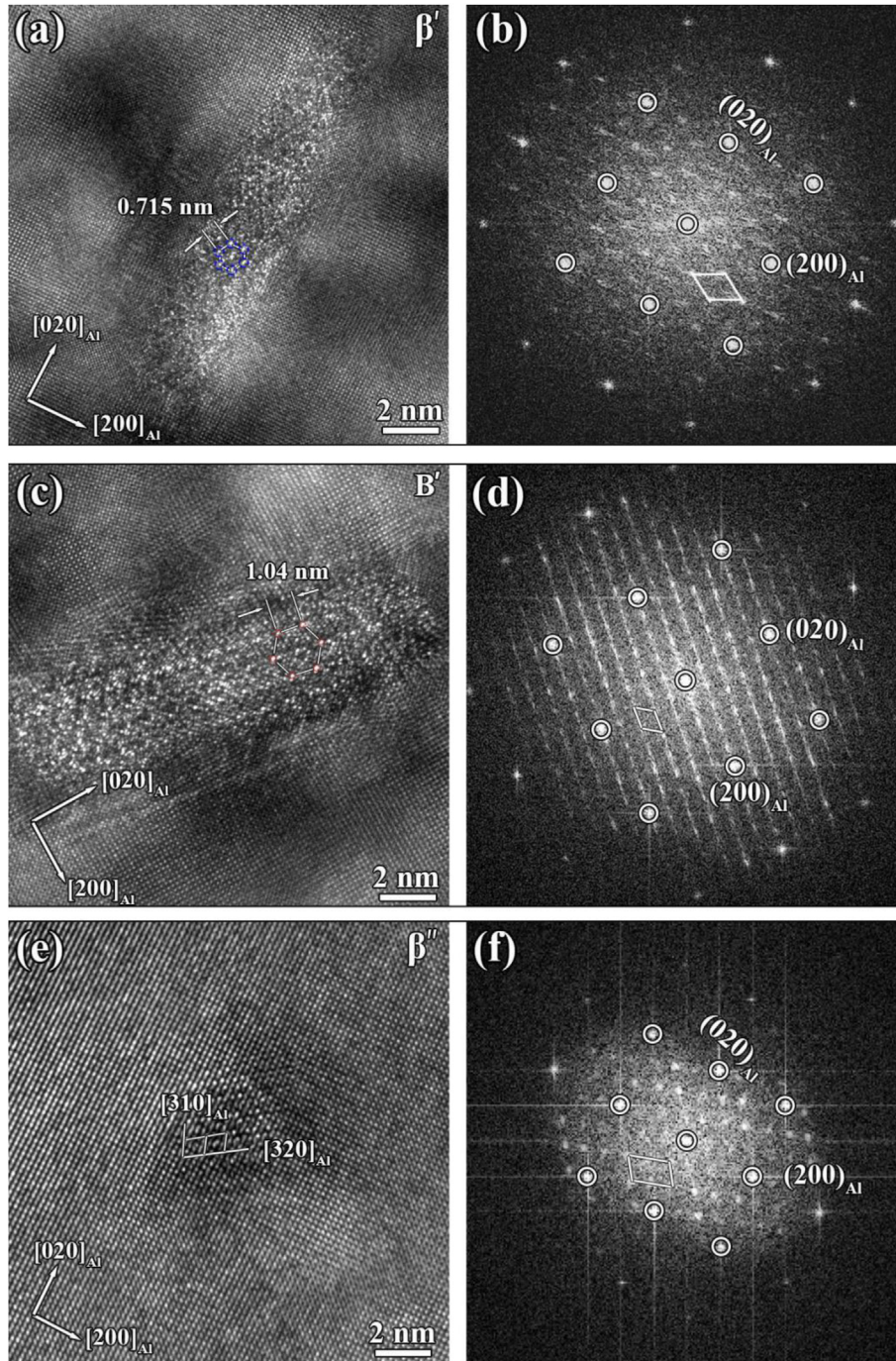
Fig. 12 — HRTEM images and corresponding FFT patterns of three typical precipitates: (a), (b) β' phase; (c), (d) B′ phase; (e), (f) β'' phase.

Al−Mg−Si alloy by Liu et al. [33] and could be explained by the following equations [33,34]:

$$N = Z\beta^* N_c \exp\left(-\frac{\Delta G^*}{k_B T}\right) \tag{1}$$

$$\Delta G^* = \frac{f\gamma^3}{F^2} \tag{2}$$

where the N refers to the nucleation rate, Z is the Zeldovich factor, β^* is the atomic attachment rate, N_c is the number of the available nucleation sites, k_B is the Boltzmann constant, ΔG^* is the nucleation energy barrier, γ is the interfacial energy, f is a constant of homogeneous nucleation, and F is the driving force mainly deriving from super-saturation. The N could be enhanced by an increasing temperature and an increasing F.

In the present work, the peak temperature of the thermal cycles in the LHZ was higher than conventional artificial aging temperature of an Al−Mg−Si alloy, which facilitated the movement of atoms. Moreover, the re-dissolved solute atoms

improved the driving force beyond the nucleation energy barrier, and promoted the formation of β' phase directly based on the Mg-rich clusters [33], where the formation of B' was due to the diffusion of Si atoms. Finally, when subjected to the PWAA, a large number of β'' precipitates re-precipitated deriving from the re-dissolved solute atoms in the matrix to contribute to the hardness increment in the LHZ and induced the UTS enhancement of the T4-BT joint strikingly.

In summary, the precipitate morphology control in the LHZ could be achieved by the selection of the original state of the plates, optimizing of welding parameters and PWAA. The original state of the plates determined the original status of the precipitates, and the welding parameters and PWAA would decide the evolution behaviors of the precipitates. Given a proper PWAA process, the LHZ of T4-BT joint could exhibit a similar enhancing ability as the NZ, and much higher than that of the T6-BT joint with the ultimate tensile strength increased by ~11.4%. The concept will provide guidance for improving the strength of the BT-FSW Al–Mg–Si joints in engineering applications.

5. Conclusions

In the present work, the microstructure control in the LHZs of the BT-FSW Al–Mg–Si joints was attempted. The basic differences among T4-BT, T4-BT-PWAA and T6-BT joints were revealed from microstructural perspective with more efforts on the microstructure evolution in the LHZs of the joints. The following conclusions are drawn:

(1) The microstructure control of a BT-FSW Al–Mg–Si joint was achieved with a proposed process: the plates were welded under T4 condition followed by PWAA.
(2) For the T6-BT joint, the LHZ exhibited an over-aging condition characterized by high density of β' phase. The limited increment of the hardness values (~6 HV) was due to the precipitation coarsening in the LHZ.
(3) For the T4-BT joint, the LHZ consisted of low density of precipitates with excellent re-precipitation ability. With prolonging the aging time, fine β'' phase re-precipitated to contribute to the enhancement of joint strength.
(4) The LHZ of the T4-BT joint presented a remarkable hardness increment (~17 HV) after PWAA compared to its T6 counterpart (~6 HV). The UTS of T4-BT, T6-BT and T4-BT-PWAA joints was 207 MPa, 211 MPa and 235 MPa, i.e. the UTS of the T4-BT joint had an apparent increment after PWAA.

Declaration of competing interest

The authors declare that they have no known competing financial interests or personal relationships that could have appeared to influence the work reported in this paper.

REFERENCES

[1] Mishra RS, Ma ZY. Friction stir welding and processing. Mater Sci Eng R 2005;50:1–78.
[2] Wang BB, Xue P, Xiao BL, Wang WG, Liu YD, Ma ZY. Achieving equal fatigue strength to base material in a friction stir welded 5083-H19 aluminium alloy joint. Sci Technol Weld Join 2019;25:81–8.
[3] Wu LH, Xiao BL, Ni DR, Ma ZY, Li XH, Fu MJ, et al. Achieving superior superplasticity from lamellar microstructure of a nugget in a friction-stir-welded Ti–6Al–4V joint. Scr Mater 2015;98:44–7.
[4] Xue P, Ma ZY, Komizo Y, Fujii H. Achieving ultrafine-grained ferrite structure in friction stir processed weld metal. Mater Lett 2016;162:161–4.
[5] Li GH, Zhou L, Luo SF, Dong FB, Guo N. Microstructure and mechanical properties of bobbin tool friction stir welded ZK60 magnesium alloy. Mater Sci Eng:A 2020;776:138953.
[6] Sahu PK, et al. Assessment of self-reacting bobbin tool friction stir welding for joining AZ31 magnesium alloy at inert gas environment. J Magn Alloys 2019;7:661–71.
[7] Li GH, Zhou L, Luo SF, Dong FB, Guo N. Quality improvement of bobbin tool friction stir welds in Mg-Zn-Zr alloy by adjusting tool geometry. J Mater Proc Technol 2020;282:116685.
[8] Fuse K, Badheka V. Effect of shoulder diameter on bobbin tool friction stir welding of AA 6061-T6 alloy. Mater Today 2021;42(2021):810–5.
[9] Wu D, Li WY, Liu XC, Gao YG, Wen Q, Vairis A. Effect of material configuration and welding parameter on weld formability and mechanical properties of bobbin tool friction stir welded Al-Cu and Al-Mg aluminum alloys. Mater Char 2021;182:111518.
[10] Esmaily M, Mortazavi N, Osikowicz W, Hindsefelt H, Svensson JE, Halvarsson M, et al. Bobbin and conventional friction stir welding of thick extruded AA6005-T6 profiles. Mater Des 2016;108:114–25.
[11] Xu WF, Luo YX, Zhang W, Fu MW. Comparative study on local and global mechanical properties of bobbin tool and conventional friction stir welded 7085-T7452 aluminum thick plate. J Mater Sci Technol 2018;34:173–84.
[12] Trueba L, Torres MA, Johannes LB, Rybicki D. Process optimization in the self-reacting friction stir welding of aluminum 6061-T6. Int J Material Form 2018;11:559–70.
[13] smaily ME, Mortazavi N, Osikowicz W, Hindsefelt H, Svensson JE, Halvarsson M, et al. Corrosion behaviour of friction stir-welded AA6005-T6 using a bobbin tool. Corrosion Sci 2016;111:98–109.

[14] Feng JC, Li YP, Gong WB, Sun DQ. The microstructures and mechanical properties of underwater bobbin tool friction stir welded 6082-T6 aluminum alloy. Int J Adv Manuf Technol 2022;121:1443—53.

[15] Li YP, Sun DQ, Gong WB, Liu L. Effects of post-weld aging on the microstructure and properties of bobbin tool friction stir-welded 6082-T6 aluminum alloy. Int J Miner Metall Mater 2019;26:849—57.

[16] Yang C, Ni DR, Xue P, Xiao BL, Wang W, Wang KS, et al. A comparative research on bobbin tool and conventional friction stir welding of Al-Mg-Si alloy plates. Mater Char 2018;145:20—8.

[17] Baghdadi AH, Sajuri Z, Omar MZ, Rajabi A. Friction stir welding parameters: impact of abnormal grain growth during post-weld heat treatment on mechanical properties of Al-Mg-Si welded joints. Metals 2020;10:1607.

[18] Malopheyev S, Vysotskiy I, Kulitskiy V, Mironov S, Kaibyshev R. Optimization of processing-microstructure-properties relationship in friction-stir welded 6061-T6 aluminum alloy. Mater Sci Eng 2016;662:136—43.

[19] Sato YS, Urata M, Kokawa H. Parameters controlling microstructure and hardness during friction-stir welding of precipitation-hardenable aluminum alloy 6063. Metall Mater Trans A 2002;33:625—35.

[20] Yang MJ, Orekhov A, Hu ZY, Feng M, Jin SB, Sha G, et al. Shearing and rotation of β'' and β' precipitates in an Al-Mg-Si alloy under tensile deformation: in-situ and ex-situ studies. Acta Mater 2021;220:117310.

[21] Ding LP, Jia ZH, Zhang ZQ, Sanders RE, Liu Q, Yang G. The natural aging and precipitation hardening behaviour of Al-Mg-Si-Cu alloys with different Mg/Si ratios and Cu additions. Mater Sci Eng:A 2015;627:119—26.

[22] Zhu SQ, Shih HC, Cui XY, Yu CY, Ringer SP. Design of solute clustering during thermomechanical processing of AA6016 Al—Mg—Si alloy. Acta Mater 2021;203:116455.

[23] Chen HN, Lu JB, Kong Y, Li K, Yang T, Meingast A, et al. Atomic scale investigation of the crystal structure and interfaces of the B' precipitate in Al-Mg-Si alloys. Acta Mater 2020;185:193—203.

[24] Xu ZZ, Liu CY, Zhang B, Huang HF, Cheng W. Effects of base metal state on the microstructure and mechanical properties of Al—Mg—Si alloy friction stir-welded joints. J Manuf Process 2020;56:248—57.

[25] Liu FC, Ma ZY. Influence of tool dimension and welding parameters on microstructure and mechanical properties of friction-stir-welded 6061-T651 aluminum alloy. Metall Mater Trans A 2008;39:2378—88.

[26] Heinz B, Skrotzki B. Characterization of a friction-stir-welded aluminum alloy 6013. Metall Mater Trans A 2002;33:489—98.

[27] Xu XX, Yang Z, Ye YL, Wang GX, He XL. Effects of various Mg/Si ratios on microstructure and performance property of Al-Mg-Si alloy cables. Mater Char 2016;119:114—9.

[28] Osten J, Milkereit B, Schick C, Kessler O. Dissolution and precipitation behaviour during continuous heating of Al-Mg-Si alloys in a wide range of heating rates. Materials 2015;8:2830—48.

[29] Başer TA. Effect of aging parameters on the mechanical properties of naturally aged Al-Mg-Si alloy. Mater Werkst 2015;46:829—34.

[30] Li K, Song M, Du Y, Zhang H. Simulation of the electron diffraction patterns from needle/rod-like precipitates in Al—Mg—Si alloys. Mater Char 2011;62:894—903.

[31] Sunde JK, Marioara CD, Holmestad R. The effect of low Cu additions on precipitate crystal structures in overaged Al-Mg-Si(-Cu) alloys. Mater Char 2020;160:110087.

[32] Meada T, Kaneko K, Namba T, Koshino Y, Sato Y, Teranish R, et al. Structural and compositional study of precipitates in under-aged Cu-added Al-Mg-Si alloy. Sci Rep 2019. https://doi.org/10.1038/s41598-018-35134-8.

[33] Liu CH, Lai YX, Chen JH, Tao GH, Liu LM, Ma PP, et al. Natural-aging-induced reversal of the precipitation pathways in an Al—Mg—Si alloy. Scr Mater 2016;115:150—4.

[34] Kozeschnik E, Svoboda J, Fratzl P, Fischer F. Modelling of kinetics in multi-component multi-phase systems with spherical precipitates-II: numerical solution and application. Mater Sci Eng:A 2004;385:157—65.